

Decoder Performance in Hybrid CV-Discrete Surface-Code Threshold Estimation Using LiDMaS+

Dennis Delali Kwesi Wayo ^{1,2} Chinonso Onah,^{3,4} Vladimir Milchakov ⁵ Leonardo Goliatt, ⁶ and Sven Groppe, ⁷

¹College of Computing, Georgia Institute of Technology, Atlanta, GA 30332 USA

²Independent Quantum Architecture Researcher & Software Developer, SchroSIM Quantum Software Project*

³Volkswagen AG, Berliner Ring 2, Wolfsburg 38440, Germany

⁴Department of Physics, RWTH Aachen, Germany[†]

⁵Apex Qubits, Paris, France[‡]

⁶Department of Computational and Applied Mechanics, Federal University of Juiz de Fora, Juiz de Fora, 36036-900, Brazil[§]

⁷Institute of Information Systems, University of Lübeck, 23562 Lübeck, Germany[¶]

(Dated: March 10, 2026)

Threshold estimation is central to fault-tolerant quantum computing, but the reported threshold depends not only on the code and noise model, but also on the decoder used to interpret syndrome data. We study this dependence for surface-code threshold estimation under both a standard Pauli noise model and a hybrid continuous-variable/discrete model motivated by GKP-style digitization. Using LiDMaS+ as a common experimental platform, we compare minimum-weight perfect matching (MWPM) and Union-Find under matched sweep grids, matched distances, and deterministic seeding, and we additionally evaluate trained neural-guided MWPM in the hybrid regime. In the Pauli baseline at distance $d = 5$, MWPM consistently outperforms Union-Find, reducing the mean sampled logical error rate from 0.384 to 0.260, and producing a stable threshold summary with crossing median $p_c \approx 0.053$. In the hybrid fixed-distance run, Union-Find is substantially worse than MWPM (mean LER 0.1657 versus 0.1195), while trained neural-guided MWPM tracks MWPM closely (mean LER 0.1158). Across hybrid multi-distance sweeps, the distance-dependent reversal in logical-error ordering remains visible, but the grid-based crossing estimator still returns boundary-valued $\sigma_c = 0.05$ for all decoders. Neural-guided runs also show elevated decoder-failure diagnostics at high noise (max decoder-failure rate 0.1335 at $d = 7, \sigma = 0.60$), indicating that learned guidance quality and decoder robustness must be reported alongside threshold curves. These results show that decoder choice and estimator design both materially affect threshold inference.

I. INTRODUCTION

Threshold estimation remains one of the central quantitative tools in fault-tolerant quantum computing because it connects a physical noise model to an architecture-level question: whether increasing code distance actually improves logical reliability [1]. In practice, however, a threshold is not a purely abstract property of a code family. It is an operational quantity extracted from a simulation pipeline that includes a noise model, a syndrome-generation procedure, a decoder, and a finite statistical estimator. For that reason, threshold claims must be interpreted not only through the code and the noise channel, but also through the decoding procedure used to turn syndrome data into corrections.

This issue becomes especially important in hybrid continuous-variable/discrete settings motivated by Gottesman-Kitaev-Preskill style encodings and related oscillator-based architectures [2–4]. In such settings, the underlying physical disturbance is naturally described as a continuous-variable displacement process, but the

threshold analysis is ultimately carried out through digitized syndrome information and discrete decoder actions. That transition from continuous noise to decoder-facing discrete data raises a methodological question that is easy to overlook: does decoder choice continue to matter in the same way that it does in a standard Pauli study, or does the hybrid noise model alter the visibility and stability of decoder-dependent effects?

Matching-based decoding remains a strong practical reference point for surface-code studies [5], while Union-Find offers a lower-cost approximate alternative with attractive scaling properties [6]. Both are scientifically relevant, but for different reasons. MWPM is valuable because it often sets the accuracy-oriented baseline. Union-Find is valuable because it tests whether a cheaper decoder preserves the same scientific conclusions. If both decoders lead to the same logical-error trends and threshold summaries, then the threshold inference is comparatively robust. If they do not, then decoder choice is not merely an implementation detail; it is part of the meaning of the reported threshold itself.

This paper presents a controlled decoder-comparison study of surface-code threshold estimation under both Pauli and hybrid CV-discrete noise using LiDMaS+ as the common experimental platform. We compare MWPM and Union-Find under matched sweep grids, matched distances, and deterministic seeding, and we include trained neural-guided MWPM in the hybrid sweeps. The results

* dwayo3@gatech.edu

† calistusnonso@gmail.com

‡ vladimir.milchakov@gmail.com

§ goliatt@gmail.com

¶ sven.groppe@gmx.de

show a clear decoder separation in the Pauli baseline, where MWPM consistently outperforms Union-Find and yields a more stable threshold summary. In the hybrid experiments, Union-Find is again clearly separated from MWPM at fixed distance and in multi-distance summaries, while neural-guided MWPM stays close to MWPM at moderate noise but develops non-negligible decoder-failure diagnostics at the highest-noise points. The main contribution of the paper is therefore methodological as much as numerical: it demonstrates that decoder choice can materially affect threshold inference in both discrete and hybrid settings, and that hybrid threshold claims require decoder diagnostics, careful sweep resolution, and estimator-aware interpretation.

A. Research Contributions

This study is guided by three linked questions. First, does decoder choice materially change threshold behavior when noise is generated as continuous-variable Gaussian displacement and then digitized into effective Pauli faults in the GKP spirit [2]? Second, is decoder ranking stable across distance scaling ($d = 3, 5, 7$), rather than only at a single distance? Third, how sensitive are practical threshold summaries to the combined choice of decoder and estimator in finite Monte Carlo sweeps [5, 6]?

The contributions follow directly from these questions. We provide a reproducible LiDMaS+ comparison protocol with matched seeds, grids, and outputs across MWPM, Union-Find, and trained neural-guided MWPM. We report paired Pauli-baseline and hybrid CV-discrete results so hybrid behavior can be interpreted against a standard reference. We include decoder-failure diagnostics alongside LER and threshold summaries, and we present an estimator-aware interpretation of crossing behavior to separate stable decoder effects from grid- or method-induced artifacts.

B. Background and Related Work

Surface-code studies commonly report logical-error curves, curve crossings, and finite-size scaling summaries to evaluate whether larger distance improves reliability [1]. A persistent comparability issue is that these summaries depend on the decoder and estimator stack used to produce them, even when the underlying code family is unchanged.

Matching-based decoding remains one of the strongest practical reference points for surface-code benchmarking. Modern implementations such as sparse-blossom style matching provide high-quality decoding while remaining computationally tractable for large simulation campaigns [5]. For that reason, MWPM is a natural accuracy-oriented baseline in any decoder-comparison study. Union-Find occupies a different but equally important role. It offers an almost-linear-time approximate

alternative that is attractive when parameter sweeps become large, but approximation can matter scientifically if it changes the resulting logical-error curves or the stability of threshold extraction [6]. A central motivation of the present paper is therefore not simply to rank decoders, but to ask whether replacing a stronger decoder by a cheaper one changes the threshold story itself.

Learned or neural-guided decoding approaches add a further dimension to this discussion by attempting to preserve strong decoding quality while reducing search or improving weighting heuristics. Such approaches are relevant because they illustrate that decoder design is an active modeling choice rather than fixed infrastructure. However, learned decoders are only as informative as the quality and scope of the model used to guide them. For that reason, learned comparisons should be accompanied by explicit model provenance and robustness diagnostics. In this study, we therefore report decoder-failure statistics alongside neural-guided LER curves.

The hybrid CV-discrete setting introduces an additional layer of interest. GKP-style encodings and related photonic proposals motivate noise models in which the underlying disturbance is continuous-variable, while correction is ultimately organized through digitized syndrome data and discrete decoder actions [2–4]. That regime is important because it sits between oscillator-level physical realism and the discrete abstractions used in threshold studies. The present comparison is therefore worthwhile precisely because it tests whether decoder dependence remains visible after this CV-to-discrete translation, or whether the hybrid regime changes the practical interpretation of threshold summaries.

Recent peer-reviewed developments in decoder and code design include XZZX-oriented and bias-tailored strategies, scalable parallel decoders, and gate-oriented fault-tolerant refinements [7–17]. These works provide the broader methodological context for studying decoder-dependent threshold behavior in a controlled simulation framework.

On the experimental side, recent demonstrations across superconducting, silicon-spin, and bosonic platforms report progressively stronger logical protection and below-threshold operation [18–25]. Related studies on logical-noise mitigation and high-threshold memory constructions further inform practical fault-tolerant design choices [26–28].

C. LiDMaS+ as the Experimental Platform

LiDMaS+ is used here as an experimental platform rather than as the subject of a software description. For the purposes of this paper, its main value is that it exposes a consistent surface-code threshold workflow across multiple decoders and noise modes while keeping the run configuration explicit and reproducible. The experiments reported here all invoke the same threshold-oriented code path, centered on the `--surface.threshold` workflow, with decoder choice, distance set, sweep window, trial

count, and output location supplied as run-time arguments. This matters because it keeps the decoder comparison inside one implementation framework instead of spreading it across incompatible tools or ad hoc scripts.

The compared decoders are accessed through the same LiDMaS+ decoder interface, which allows MWPM, Union-Find, and neural-guided MWPM to be swapped without changing the surrounding experiment logic. In practice, this means that the differences reported in the paper can be attributed to decoder behavior rather than to differences in file formats, sweep construction, or post-processing conventions. The paper-specific workflows used in this study call the compiled LiDMaS+ binary from shell scripts that generate fixed-distance baselines, multi-distance sweeps, and threshold-oriented runs under matched settings.

Reproducibility is supported through deterministic seeding, fixed sweep grids, and structured outputs. Each run records the chosen seed, the decoder, the distance, the physical-noise parameter, the number of trials, and the resulting logical error statistics in machine-readable tabular form. The reported outputs also include confidence intervals and auxiliary decoder diagnostics such as defect and weight summaries, which makes it possible to reproduce both the figures and the threshold summary tables from the saved artifacts rather than from hand-copied numbers. For threshold-oriented Pauli runs, LiDMaS+ further emits scaling reports and JSON summaries used to construct the finite-size table. In the hybrid case, the same tabular outputs support a more conservative crossing analysis derived directly from the sampled curves.

The specific execution path used in the paper is the dedicated `paper_runs/` workflow added on top of the repository examples. That layer does not alter the decoding logic. It standardizes the experiment matrix, output directories, merged tabular-data generation, and publication-figure rendering. This separation is useful because it keeps the scientific workflow explicit and auditable while preserving LiDMaS+ itself as the common simulation backend. In that sense, LiDMaS+ is suitable for the present study not because it automates every possible analysis, but because it provides a stable and decoder-consistent environment in which methodological differences can be isolated and compared.

II. METHODOLOGY

This section defines the end-to-end workflow used to generate all results. The methodology is intentionally closed-loop and reproducible: seeds, sweep grids, and trial budgets are fixed so decoder effects can be isolated under matched conditions. For each operating point, LiDMaS+ samples noise, extracts syndrome data, runs one decoder backend, applies correction, and records logical failures. The pipeline then computes logical error rates with confidence intervals, aggregates distance-dependent curves, and performs threshold-oriented analysis in mode-

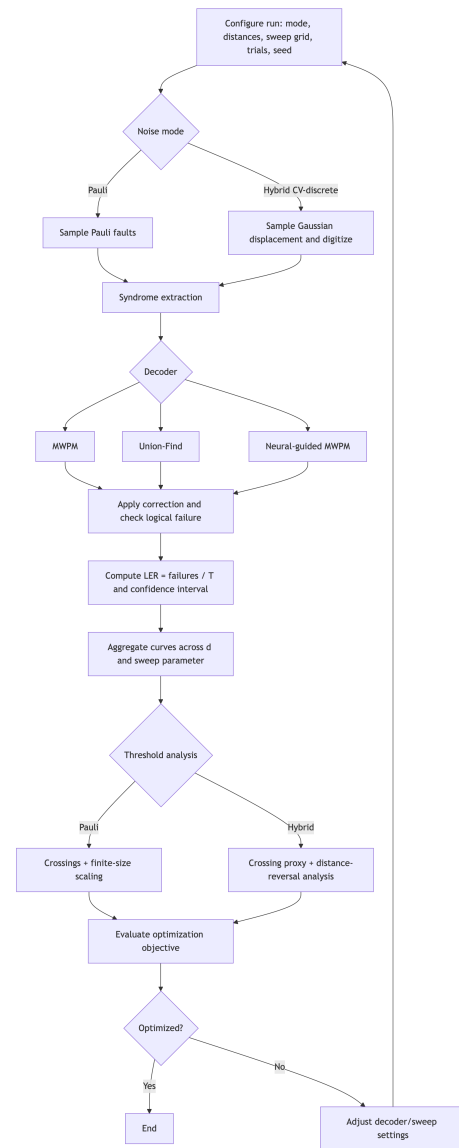


Figure 1. Closed-loop LiDMaS+ methodology used in this study. The run branches by noise mode and decoder, recombines for LER estimation and threshold analysis, and then evaluates optimization status. If settings are not optimized, the process loops back to reconfigure and rerun under the same reproducibility controls.

specific branches. A final optimization decision controls whether settings are adjusted and rerun or accepted as final. Figure 1 summarizes this full process.

A. Noise Models

The study uses two noise models implemented in LiDMaS+. The first is a Pauli baseline used to anchor interpretation against the standard surface-code literature [1]. In this mode, the physical sweep variable is the Pauli error rate p , and the resulting threshold analysis can be read

in the familiar language of logical error curves, crossings, and finite-size scaling. The Pauli mode is not the main novelty of the paper, but it is methodologically important because it provides a controlled reference in which the expected distinction between a stronger matching-based decoder and a cheaper approximate decoder should be visible if the comparison protocol is working correctly.

The second and primary model is the hybrid CV-discrete noise channel. In this setting, the physical sweep variable is the Gaussian displacement scale σ , and the simulator converts the underlying continuous-variable disturbance into effective discrete correction events in the Gottesman-Kitaev-Preskill spirit [2]. This hybrid model is the regime of interest because it links oscillator-level noise intuition to the decoder-facing syndrome data that enter a surface-code threshold calculation. Throughout the paper, the hybrid mode is treated as the main scientific setting, while the Pauli mode is used as a baseline for interpreting whether decoder-dependent effects survive the transition from purely discrete faults to digitized CV noise.

B. Decoders Compared

The comparison focuses on minimum-weight perfect matching (MWPM), Union-Find, and neural-guided MWPM. MWPM is the high-quality reference decoder and is the natural baseline for threshold studies because matching-based decoding remains one of the strongest practical standards for surface-code syndrome processing [5]. In the present study, MWPM is treated as the accuracy-oriented reference against which other decoders are judged.

Union-Find is included as the principal approximate alternative [6]. Its importance is methodological rather than merely algorithmic: it tests whether a lower-cost decoder preserves the same threshold conclusions as a stronger matching-based backend, or whether the decoder approximation itself changes the reported logical-error trends and practical crossing summaries. This question is central to the paper because a threshold estimate is only as reliable as the inference procedure that produced it.

Neural-guided MWPM is evaluated using a trained linear guidance model (generated by the project training workflow) rather than the earlier demonstration-only dummy model. We include this decoder in the hybrid experiments to test whether learned edge reweighting changes practical threshold behavior under matched seeds and grids. At the same time, we treat neural outputs with explicit caution by reporting decoder-failure diagnostics together with logical-error metrics, because guidance quality and decoder robustness can decouple at high-noise points.

Algorithm 1: Surface-code threshold run (generic decoder)

Input: Decoder D , mode m , distances \mathcal{D} , sweep grid \mathcal{S} , trials T , base seed s_0
Output: Logical-error estimates and confidence intervals for each (d, θ) point

```

foreach  $d \in \mathcal{D}$  do
  foreach  $\theta \in \mathcal{S}$  do
    failures  $\leftarrow 0$ 
    for  $t = 1$  to  $T$  do
      Set RNG seed from  $(s_0, d, \theta, t)$ 
      Sample physical noise under  $(m, \theta)$  and
      extract syndrome  $y_t$ 
       $c_t \leftarrow \text{Decode}_D(y_t, d)$ 
      if  $c_t$  yields a logical failure then
        failures  $\leftarrow$  failures + 1
    Record  $\text{LER}(d, \theta) = \text{failures}/T$  and CI

```

C. Threshold Estimation Protocol

All experiments follow the same basic protocol. For a chosen decoder, code distance, and point on the physical-noise sweep, LiDMaS+ generates repeated noisy samples, performs syndrome extraction and decoding, and records whether each trial results in a logical failure. The logical error rate is then estimated as the empirical failure frequency at that operating point, and the simulator reports accompanying confidence intervals in the output tables. This procedure is repeated across a matched sweep grid for every decoder so that each curve comparison is pointwise aligned in both noise parameter and trial count.

Threshold-oriented analyses are built on top of this same data-generation loop. In the Pauli setting, we use the built-in threshold-estimation and finite-size-scaling routines to obtain pairwise crossings, an aggregate crossing median, and a collapse-based estimate of the critical point together with a bootstrap-derived uncertainty range. In the hybrid setting, we again use matched multi-distance sweeps, but the present analysis emphasizes practical crossing behavior rather than a strong asymptotic threshold claim. This distinction is deliberate: the hybrid data in the current grid are sufficiently informative to show distance reversal, but not yet sufficiently resolved to support a more ambitious universality-style inference.

D. Algorithmic Summary

For implementation clarity, Algorithms 1–4 summarize the full threshold loop and the three decoders used in this paper.

Algorithm 2: MWPM surface decoder

Input: Syndrome graph $G = (V, E)$, boundary set ∂V , edge weights w
Output: Surface correction c
 Build matching instance with pair and boundary edges
 Assign edge and boundary costs from w
 $M \leftarrow \text{BlossomSolve}(G, w)$
 Initialize correction bitmask $c \leftarrow 0$
foreach *matched pair* $(u, v) \in M$ **do**
 | Route minimum-weight path $P(u, v)$
 | Toggle qubits along $P(u, v)$ in c
 Verify syndrome consistency $Hc = y \pmod{2}$
return c

Algorithm 3: Union-Find surface decoder

Input: Defect set \mathcal{X} on lattice L
Output: Surface correction c
 Initialize one odd cluster per defect
while *an odd cluster exists* **do**
 | Grow each odd-cluster frontier by one edge
 | Merge clusters on frontier collisions
 | Attach a cluster to boundary when reached
 Build spanning forest in each merged cluster
 Peel leaves to satisfy parity and mark correction flips in c
 Verify syndrome consistency
return c

E. Metrics

The primary metric throughout the paper is the logical error rate (LER). This is the quantity plotted in the fixed-distance and multi-distance figures, and it is the metric from which all threshold-oriented summaries are derived. Confidence intervals are used to judge whether observed curve separations are likely to reflect a real decoder effect rather than pure sampling noise. For the Pauli threshold study, we additionally report crossing estimates, collapse-based critical-point estimates, the fitted exponent ν , and the collapse cost returned by the scaling routine. For the hybrid threshold study, we report decoder-labeled crossing proxies derived from the sampled multi-distance curves, while explicitly noting when those summaries are limited by grid resolution.

We do not report runtime as a formal metric in this paper. That omission is intentional. The present study is designed to answer a decoding-quality question, namely whether decoder choice changes logical-error trends and threshold summaries, not to produce a hardware-normalized performance benchmark. A runtime comparison can be added in future work, but only if it is measured under fixed hardware and reproducible execution controls.

Algorithm 4: Neural-guided MWPM surface decoder

Input: Defects \mathcal{X} , trained model f_ϕ , base matching weights w
Output: Guided correction c and decoder-failure diagnostic if needed
foreach *defect pair* (i, j) **do**
 | Extract features x_{ij} (distance and boundary-aware terms)
 | $\alpha_{ij} \leftarrow \text{Clip}(f_\phi(x_{ij}))$
 | $\tilde{w}_{ij} \leftarrow \alpha_{ij} \cdot w_{ij}$
foreach *defect* i **do**
 | Compute guided boundary weight $\tilde{w}_{i,\partial}$
 Solve MWPM on guided weights \tilde{w} and lift to correction c
if *syndrome verification fails* **then**
 | Emit decoder-failure diagnostic
return c

III. EXPERIMENTAL DESIGN

The experiments were designed around a small number of tightly controlled comparisons rather than a broad benchmark catalogue. The goal was to answer three concrete questions: whether MWPM and Union-Find separate clearly in a familiar Pauli setting, whether that separation survives in the hybrid CV-discrete regime, and how trained neural-guided MWPM behaves relative to both under matched conditions. To make those comparisons one-to-one, we used deterministic seeding, identical sweep grids across decoders, and a common machine-readable tabular output format throughout the campaign. The full run matrix used in the paper is summarized in Table I.

The first layer of the design is a fixed-distance baseline. We chose distance $d = 5$ because it is large enough to show nontrivial logical behavior while remaining inexpensive enough for repeated matched sweeps. The Pauli baseline uses $p \in [0.03, 0.12]$ with step size 0.01 and 3000 trials per point. This experiment is not the centerpiece of the paper, but it is essential as an interpretive anchor because it tests whether the workflow recovers the expected advantage of a stronger matching-based decoder in a standard discrete setting.

The second fixed-distance experiment uses the same distance and sweep structure, but replaces the Pauli sweep by a hybrid sweep over $\sigma \in [0.05, 0.60]$ with step size 0.05 and includes MWPM, Union-Find, and neural-guided MWPM. This is the central comparison implied by the title of the paper. The point of this run is not simply to reproduce the Pauli benchmark under a different parameter name. It is to determine whether a decoder gap that is visible in a discrete setting remains visible once the underlying noise begins as a continuous-variable displacement process and is only later interpreted through a discrete correction interface.

The second layer of the design introduces distance scal-

Table I. Experimental matrix for the decoder-comparison study (seed 1337; common LiDMaS+ workflow).

Run	Mode	d	Sweep	Trials	Purpose
Pauli baseline	Pauli	5	$p \in [0.03, 0.12]$, 0.01	3000	Decoder comparison (fixed d)
Hybrid baseline	Hybrid	5	$\sigma \in [0.05, 0.60]$, 0.05	2000	Decoder comparison (fixed d)
Hybrid multi- d	Hybrid	3,5,7	$\sigma \in [0.05, 0.60]$, 0.05	2000	Distance scaling trends
Pauli threshold	Pauli	3,5,7	$p \in [0.04, 0.12]$, 0.01	2000	Crossings / FSS
Hybrid threshold	Hybrid	3,5,7	$\sigma \in [0.05, 0.60]$, 0.05	2000	Crossing proxy; reversal

ing. For this purpose, we ran a hybrid multi-distance sweep at $d = 3, 5, 7$ using the same σ window and the same three-decoder set. This run is the basis of the main distance-dependent figure because it reveals where the ordering of the logical-error curves reverses as the noise strength increases. It also provides the raw material for the hybrid crossing summary. We deliberately prioritized multiple distances because a decoder comparison at one distance cannot support a threshold-oriented claim on its own.

The final layer of the design consists of two threshold-focused runs. In the Pauli case, we used $d = 3, 5, 7$, a sweep window $p \in [0.04, 0.12]$ with step size 0.01, 2000 trials per point, and the built-in threshold-estimation and finite-size-scaling routines with 100 bootstrap samples. This produces pairwise crossings, an aggregate crossing median, and collapse-fit summaries for both Pauli decoders (MWPM and Union-Find). In the hybrid case, we used the analogous $d = 3, 5, 7$ configuration over $\sigma \in [0.05, 0.60]$ with step size 0.05 and 2000 trials per point for all three hybrid decoders. The hybrid run is used more cautiously. It supports a practical crossing proxy and a distance-reversal analysis, but not yet a strong asymptotic threshold claim, because the current grid is too coarse and the low-noise plateau is too long.

This design leads directly to the figure and table structure used in the paper. The fixed-distance Pauli and hybrid runs supply the baseline comparison figure. The hybrid multi-distance run supplies the main scaling-style figure together with a decoder-labeled summary table. The Pauli threshold run supplies the finite-size summary table, while the hybrid threshold run supplies a practical crossing-summary table derived from the sampled data.

IV. RESULTS

We now report the decoder-comparison results obtained from the fixed-distance baseline experiments, the multi-distance hybrid sweeps, and the threshold-oriented Pauli and hybrid analyses. All fixed-distance and multi-distance curve comparisons were generated with deterministic seeds and matched sweep grids. The Pauli baseline figure uses 3000 trials per point, while the hybrid baseline, hybrid multi-distance, and threshold-oriented runs use 2000 trials per point (with 100 bootstrap samples for the Pauli scaling analysis). The main empirical message is that decoder choice clearly matters in the Pauli baseline and remains

visible in the hybrid setting: Union-Find degrades relative to MWPM, while trained neural-guided MWPM stays close to MWPM at moderate noise but shows elevated decoder-failure diagnostics at the highest-noise points.

A. Baseline Decoder Comparison

The clearest decoder separation appears in the Pauli baseline at fixed distance $d = 5$, shown in Fig. 2(a). Across the full sweep window $p \in [0.03, 0.12]$, MWPM yields a lower logical error rate than Union-Find at every sampled point. At the low-noise end, MWPM gives LER = 0.056 at $p = 0.03$, whereas Union-Find gives LER = 0.130. The separation remains substantial through the middle of the sweep, for example 0.141 versus 0.260 at $p = 0.05$ and 0.274 versus 0.436 at $p = 0.08$, and it persists at the high-noise end, where the corresponding values are 0.479 and 0.602 at $p = 0.12$. In aggregate, the mean logical error rate over the sampled grid is 0.260 for MWPM and 0.384 for Union-Find, while the area-under-curve proxy extracted from the sampled points is 0.0233 for MWPM and 0.0347 for Union-Find. In other words, within this discrete reference setting, MWPM reduces the sampled logical-error burden by roughly one third relative to Union-Find.

This difference is not a marginal fluctuation produced by finite sampling. The confidence intervals remain clearly separated at representative low-, mid-, and high-noise points, which means that the observed ranking is statistically visible even without a more elaborate significance analysis. The Pauli baseline therefore supports a strong first conclusion: when the noise model is purely discrete and the code distance is fixed, MWPM is the more reliable decoder of the two under the present protocol. That result is important because it provides a clean reference against which the hybrid CV-discrete behavior can be interpreted.

The hybrid fixed-distance baseline in Fig. 2(b) shows clear decoder separation at $d = 5$. On the same $\sigma \in [0.05, 0.60]$ grid, MWPM and trained neural-guided MWPM remain close to each other, while Union-Find rises substantially faster as noise increases. Representative points are $\sigma = 0.40$ (MWPM 0.0425, UF 0.101, neural 0.044), $\sigma = 0.50$ (MWPM 0.278, UF 0.421, neural 0.264), and $\sigma = 0.60$ (MWPM 0.552, UF 0.6245, neural 0.5365). The aggregate sampled summaries in Table II are consistent with this pattern: mean LER 0.1195 (MWPM),

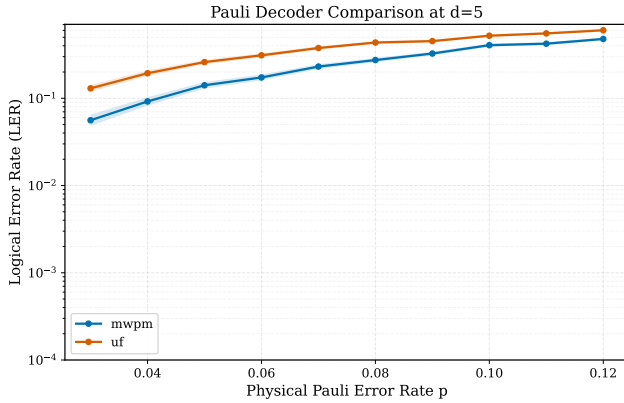
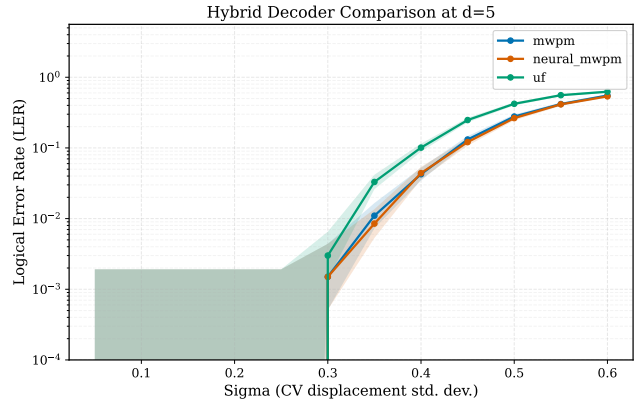
(a) Pauli baseline at $d = 5$.(b) Hybrid baseline at $d = 5$.

Figure 2. Fixed-distance decoder comparison under matched sweep settings. Panel (a) shows a clear MWPM advantage over Union-Find in the Pauli baseline. Panel (b) shows the hybrid $d = 5$ comparison with three decoders, where Union-Find is clearly separated from MWPM and trained neural-guided MWPM.

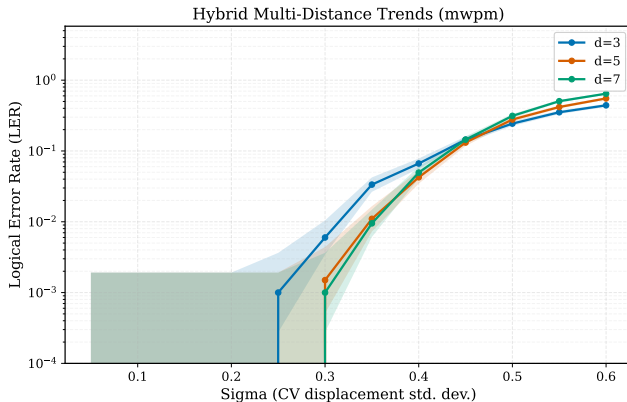


Figure 3. Hybrid multi-distance logical-error curves for $d = 3, 5, 7$ (MWPM view). The main effect is the reversal in distance ordering between the low- and high- σ regimes; decoder-to-decoder differences are summarized in Table III.

0.1657 (UF), and 0.1158 (neural), with corresponding AUC proxies 0.0579, 0.0838, and 0.0561. This indicates that decoder choice is not washed out in the present hybrid fixed-distance study.

B. Distance-Dependent Threshold Trends

The multi-distance hybrid experiment in Fig. 3 extends this comparison to $d = 3, 5, 7$ and clarifies what can and cannot be inferred from the hybrid dataset. Decoder differences are now visible and distance dependent (Table III). At $d = 3$, all decoders are close (AUC 0.0534 MWPM, 0.0527 UF, 0.0523 neural). At $d = 5$ and $d = 7$, Union-Find separates clearly upward (AUC 0.0838 and 0.1085), while neural-guided MWPM remains near MWPM in

AUC but with higher decoder-failure diagnostics at high noise for $d = 7$.

The distance trends still show a clear regime change as σ increases. In the low-noise region, all three distances remain near zero logical failure, and larger codes are at least as good as smaller ones. For MWPM, representative values are $\sigma = 0.30$ ($d = 3 : 0.006$, $d = 5 : 0.0015$, $d = 7 : 0.001$) and $\sigma = 0.40$ (0.0665, 0.0425, 0.0495). By $\sigma = 0.50$, the ordering reverses to 0.2435, 0.278, and 0.313; at $\sigma = 0.60$ it widens to 0.441, 0.552, and 0.644. Union-Find follows the same qualitative reversal but with larger high-noise LER (e.g., $d = 7, \sigma = 0.40 : 0.2035$ and $\sigma = 0.60 : 0.6935$). Neural-guided MWPM tracks MWPM closely through moderate noise, then diverges at the top end where decoder-failure diagnostics increase.

What changes relative to the Pauli baseline is not whether decoder dependence exists, but how it appears. In Pauli mode, MWPM dominates Union-Find across the whole sweep. In hybrid mode, Union-Find degradation is most visible at larger distances and moderate-to-high σ , while neural-guided MWPM stays close to MWPM in LER summaries yet exhibits robustness limits in decoder-failure diagnostics at the noisiest points. The conservative interpretation is therefore two-part: the hybrid experiment does show decoder-dependent behavior, but estimator resolution and decoder-failure effects still limit strong asymptotic threshold claims.

C. Crossing and Threshold Estimates

The threshold-oriented analyses sharpen this distinction between the Pauli and hybrid regimes. In the Pauli setting, summarized in Table IV, MWPM produces a well-defined crossing structure and a stable finite-size scaling summary. The pairwise crossing estimates occur at $p_c \approx 0.0622$ for the ($d = 3, d = 5$) pair and $p_c \approx 0.0439$

Table II. Hybrid fixed-distance summary at $d = 5$ for $\sigma \in [0.05, 0.60]$ (2000 trials/point).

Decoder	Points	Mean LER	AUC proxy	Max decoder fail rate
MWPM	12	0.1195	0.0579	0.0000
Union-Find	12	0.1657	0.0838	0.0000
Neural-MWPM (trained)	12	0.1158	0.0561	0.0010

Table III. Hybrid multi-distance summary from sampled curves (2000 trials/point).

Decoder	AUC at $d = 3$	AUC at $d = 5$	AUC at $d = 7$
MWPM	0.0534	0.0579	0.0672
Union-Find	0.0527	0.0838	0.1085
Neural-MWPM (trained)	0.0523	0.0561	0.0695

for the ($d = 3, d = 7$) pair, yielding an aggregate crossing median of 0.0531 with bootstrap interval [0.0415, 0.0572]. The corresponding collapse fit gives $p_c = 0.052$ with interval [0.040, 0.064], exponent $\nu = 1.35$, and collapse cost 8.05×10^{-5} . Taken together, these quantities indicate that the MWPM Pauli curves contain a coherent threshold signal under the present sampling protocol.

Union-Find behaves differently under the same Pauli threshold analysis. As Table IV shows, no crossings are detected on the sampled Pauli grid, and the collapse fit is pushed to the lower boundary of the search region, with $p_c = 0.040$, $\nu = 0.5$, and collapse cost 2.33×10^{-3} . The much larger collapse cost, together with the absence of detected crossings, shows that practical threshold inference is substantially less stable for Union-Find in this discrete baseline. This is an important methodological result. It means that decoder choice changes not only the logical-error curves themselves, but also whether a threshold estimate can be extracted cleanly from a finite simulation campaign.

The hybrid threshold summary in Table V must be interpreted more cautiously. A direct grid-based crossing summary for all three decoders returns $\sigma = 0.05$ for the ($d = 3, d = 5$) and ($d = 5, d = 7$) pairs. On its face, this suggests that the crossing occurs at the lower boundary of the sampled interval. However, inspection of the raw multi-distance curves in Fig. 3 and Table III shows that the qualitative reversal in distance ordering becomes operationally visible closer to $\sigma \approx 0.40$ – 0.50 . The boundary-valued summary is therefore an artifact of the present estimator interacting with the long low-noise plateau, not convincing evidence that the physical transition truly sits at $\sigma = 0.05$. For that reason, the current hybrid threshold analysis should be described as a coarse operational crossing proxy rather than as a final threshold determination. The scientifically defensible claim is that the hybrid data exhibit threshold-like distance reversal and decoder-dependent degradation (especially for Union-Find at higher distance), but that finer sweeps and stronger crossing estimators are still needed before precise decoder-dependent threshold shifts in the hybrid regime can be quantified confidently.

D. Comparison with Previous Studies

To position the present decoder-comparison results in a broader context, Table VI summarizes representative published values from APS, Nature, and Springer venues together with the corresponding LiDMaS+ outcomes. Because these studies differ in noise model (Pauli, biased-noise, and hardware-realistic), decoder assumptions, and endpoint metrics, the values should be read as contextual anchors rather than as strict one-to-one rankings.

Table VI highlights that literature values vary over orders of magnitude because each study optimizes for a different objective (proof guarantees, asymptotic thresholds under specific noise bias, or hardware cycle-level performance). The main role of the present LiDMaS+ study is therefore methodological: it isolates decoder-dependent effects and estimator sensitivity under matched runs, providing a controlled bridge between Pauli-baseline threshold analysis and hybrid CV-discrete decoding behavior.

V. DISCUSSION

The results support two different conclusions, depending on which noise regime is considered. In the Pauli baseline, MWPM is clearly the stronger decoder under the present protocol. It produces lower logical error rates across the entire fixed-distance sweep and yields a threshold analysis with identifiable crossings and a substantially better collapse fit than Union-Find. This is the clearest result in the paper, and it validates the use of the LiDMaS+ workflow as a meaningful decoder-comparison platform rather than a purely descriptive simulator.

The hybrid results are more nuanced than a simple two-decoder ranking. Union-Find now shows a clear degradation relative to MWPM at fixed distance and especially at larger distance, while trained neural-guided MWPM remains close to MWPM on LER summaries across most of the sampled regime. At the same time, neural-guided runs develop non-negligible decoder-failure diagnostics at high noise (up to 0.1335 at $d = 7, \sigma = 0.60$), which limits

Table IV. Pauli threshold and finite-size scaling summary extracted from the $d = 3, 5, 7$ runs.

Decoder	Crossing median p_c	Crossing interval	Collapse p_c	ν	Collapse cost
MWPM	0.0531	[0.0415, 0.0572]	0.0520	1.35	8.05×10^{-5}
Union-Find	N/A	–	0.0400	0.50	2.33×10^{-3}

Table V. Hybrid crossing summary derived from the sampled tabular outputs for the $d = 3, 5, 7$ runs.

Decoder	$\sigma_c(d = 3, 5)$	Method	Min. $ \Delta\text{LER} $	$\sigma_c(d = 5, 7)$	Method	Min. $ \Delta\text{LER} $
MWPM	0.05	grid exact	0	0.05	grid exact	0
Union-Find	0.05	grid exact	0	0.05	grid exact	0
Neural-MWPM (trained)	0.05	grid exact	0	0.05	grid exact	0

how strongly one should interpret neural gains from LER alone. The hybrid dataset therefore contains both decoder-dependent structure and estimator-dependent ambiguity: decoder ordering is visible, but precise crossing extraction remains sensitivity-limited by grid resolution and plateau effects.

This matters for how threshold studies should be reported. The Pauli results show that replacing the decoder can change whether a threshold estimate is cleanly extractable from finite data. The hybrid results extend that caution in two ways: decoder choice changes high-noise behavior, and coarse estimators can still return boundary-valued crossing summaries that do not faithfully represent where distance ordering reverses in raw curves. Threshold claims are therefore contingent not only on decoder identity, but also on estimator design, sweep resolution, and decoder-failure diagnostics.

Union-Find nevertheless remains scientifically useful. The present comparison does not justify treating it as interchangeable with MWPM in Pauli threshold studies, but it does show that Union-Find can still serve as a practical exploratory decoder, especially when the goal is to map out broad regions of parameter space before committing to a more expensive accuracy-oriented analysis. In future work, that makes a natural two-stage strategy: use the cheaper decoder to localize candidate transition regions, then refine the threshold analysis with MWPM or another stronger reference decoder.

The neural-guided results are informative but should be interpreted with explicit scope limits. A trained guidance model can track MWPM closely in moderate-noise regions and improve over Union-Find in sampled LER summaries, but elevated decoder-failure rates at the noisiest points show that guidance quality alone is not sufficient for robust decoding claims. Future neural comparisons should therefore report both LER and decoder-failure diagnostics as first-class outcomes.

For experimentalists and architecture researchers, the practical takeaway is straightforward. If the goal is to report a threshold or compare threshold values across studies, the decoder should be treated as part of the result, not as invisible infrastructure. Decoder identity, sweep resolution, and summary method should be reported with

the same care as code distance and noise parameters. LiDMaS+ is useful in this context because it enables those ingredients to be varied under a common workflow. The present paper therefore argues for a more careful style of threshold reporting: one in which methodological choices are made explicit and decoder dependence is tested rather than assumed away.

VI. THREATS TO VALIDITY

Several limitations constrain the strength of the conclusions. First, all reported logical-error curves are based on finite Monte Carlo samples. Although the fixed-distance runs use 3000 trials per point and the threshold-oriented runs use 2000 trials per point, uncertainty remains non-negligible in the low-error tails and near putative crossing regions. A finer estimate of small decoder differences in the hybrid regime would likely require more trials concentrated near the transition window rather than a uniform sweep budget.

Second, the study uses a limited distance range, namely $d = 3, 5, 7$ for the multi-distance and threshold-oriented analyses. This is sufficient to detect distance reversal and to perform a first scaling-style analysis, but it is not sufficient to support a strong asymptotic claim about universality or large-distance behavior. A broader distance set, including at least one higher-distance point, would strengthen any claim about decoder-dependent threshold shifts.

Third, the results depend on implementation choices within LiDMaS+, including the exact noise-to-syndrome pipeline, the threshold-estimation routines, and the current crossing heuristics. This is not a flaw of the platform, but it does mean that the reported threshold summaries should be interpreted as implementation-aligned estimates rather than decoder-agnostic truths. The hybrid crossing summary is especially sensitive to this issue because the current estimator can be dominated by a long low-noise plateau.

Fourth, the sweep windows themselves matter. The Pauli threshold analysis is restricted to $p \in [0.04, 0.12]$, and the hybrid threshold analysis to $\sigma \in [0.05, 0.60]$. If

Table VI. Contextual comparison between this work and representative published surface-code studies.

Study	Setting	Decoder	Key result
This work (LiDMaS+)	Simulated, $d = 3, 5, 7$	MWPM; Union-Find; neural-MWPM	$p_c = 0.0531$ (Pauli); $\sigma_c = 0.05$ (hybrid)
Wang (2011)[29]	Stochastic noise	Matching-style	1.1–1.4% threshold
Fowler (2012)[30]	2D NN, noisy gates	Matching proof	$p < 7.4 \times 10^{-4}$
Tuckett (2018)[31]	Biased noise	Tensor-network	43.7% (pure); 28.2% at $\eta = 10$
Tuckett (2020)[32]	Fault-tolerant bias	Bias-aware MWPM	> 6% (dephasing); $\sim 5\%$ at $\eta = 100$
Google QAI (2023)[22]	Superconducting, $d = 3, 5$	Approx. maximum likelihood	2.914% (d=5) vs 3.028% (d=3)
Google QAI (2025)[25]	Hardware to $d = 7$	Neural + real-time	$\Lambda = 2.14$; $\epsilon_7 = 1.43 \times 10^{-3}$
Lee (2021)[33]	Rectangular vs square	MWPM	Failure ratio 4.37 at $\eta = 2.5$

the physically relevant crossing lies near or outside these windows, or if the transition region is finer than the chosen step size, then the inferred threshold summary will be biased toward the sampled grid. This concern is directly relevant to the hybrid results, where the boundary-valued crossing proxy should be viewed as an estimator limitation rather than a definitive physical threshold.

Finally, although the present paper includes a trained neural-guided decoder, the model class is intentionally lightweight and was tuned within the current workflow. This makes the neural results useful for controlled internal comparison, but not yet a definitive statement about state-of-the-art learned decoding. External-model validation and cross-dataset testing remain necessary for broader neural claims.

VII. CONCLUSION AND FUTURE WORK

This paper asked whether decoder choice materially changes surface-code threshold estimation when the noise model moves from a conventional Pauli setting to a hybrid continuous-variable/discrete regime. The answer is yes, with regime-specific details. In the Pauli baseline, decoder choice clearly matters: MWPM produces lower logical error rates than Union-Find across the full sampled sweep and yields a substantially more stable threshold summary. In the hybrid experiments, decoder dependence is also visible: Union-Find degrades relative to MWPM at fixed and larger distances, while trained neural-guided MWPM remains close to MWPM in LER summaries but exhibits non-negligible decoder-failure rates at the highest-noise points. Taken together, these results show that decoder dependence is real across both regimes, and that robust threshold interpretation requires both curve metrics and decoder diagnostics.

The broader implication is methodological. Threshold values should not be treated as decoder-free properties of a code and noise model alone. They are outputs of an inference pipeline whose behavior depends on the decoding backend, the sweep window, the estimator, and the statistical budget allocated near the transition region. LiDMaS+ is useful in this context because it makes those ingredients comparable within one controlled workflow.

The next experimental step is clear. The hybrid anal-

ysis should be repeated with a finer low- σ grid, additional trial concentration near the apparent transition region, and at least one higher code distance. Beyond that, future work should broaden the decoder set, introduce stronger learned weighting models only when they are scientifically validated, and revisit the hybrid scaling analysis under tighter uncertainty control. Those extensions would convert the present paper from a careful first decoder-comparison study in the hybrid regime into a stronger threshold-estimation benchmark with more decisive asymptotic claims.

AUTHOR CONTRIBUTIONS

D.D.K.W: conceptualization, methodology, validation and visualization, software, writing – original draft, review & editing. C.O: methodology, validation and visualization, software, writing – original draft, review & editing. V.M: methodology, validation and visualization, software, writing – original draft, review & editing. L.G: methodology, validation and visualization, software, writing – original draft, review & editing. S.G: methodology, validation and visualization, software, writing – original draft, review & editing.

ACKNOWLEDGMENT(S)

The authors acknowledge contributors, users, and reviewers who provided feedback on decoding workflows, reproducibility scripts, and documentation quality. Any opinions, findings, conclusions, or recommendations expressed in this research are those of the author(s) and do not necessarily reflect the views of their respective affiliations.

DATA & CODE AVAILABILITY

The data generated and analyzed during the present study are included within the manuscript. Supplementary codes developed from LiDMaS+ simulator are provided as supplementary material and accessible on [GitHub](#) to ensure transparency and reproducibility.

FUNDING

This research was not funded.

DISCLOSURE STATEMENT

No potential conflict of interest was reported by the author(s).

Appendix A: Mathematical Formulation of the Experimental Pipeline

This appendix summarizes the equations that underlie the simulator-level workflow used in the main text.

1. Noise Models and CV-to-Discrete Mapping

In the Pauli baseline, we use a single physical error-rate parameter p and model each noisy location by

$$\mathcal{E}_p(\rho) = (1-p)\rho + \frac{p}{3}(X\rho X + Y\rho Y + Z\rho Z), \quad (1)$$

with the circuit-level implementation applying this model to each sampled fault location.

In the hybrid mode, each round samples continuous displacements in phase space,

$$\delta q, \delta p \sim \mathcal{N}(0, \sigma^2), \quad (2)$$

and applies

$$\rho \mapsto D(\delta q, \delta p)\rho D^\dagger(\delta q, \delta p), \quad (3)$$

before digitization to effective Pauli events. Let Γ_σ denote this CV-to-discrete map. Then the induced effective probabilities satisfy

$$p_I(\sigma) + p_X(\sigma) + p_Z(\sigma) + p_Y(\sigma) = 1, \quad (4)$$

where each $p_\alpha(\sigma)$ is estimated empirically from Monte Carlo samples under the same syndrome-extraction pipeline used for decoding.

2. Decoder Objectives

Let \mathcal{X} be the observed defect set and let w_{ij} be pair/boundary weights on the decoder graph.

MWPM solves

$$M^* = \arg \min_{M \in \mathcal{M}(\mathcal{X})} \sum_{(i,j) \in M} w_{ij}, \quad (5)$$

where $\mathcal{M}(\mathcal{X})$ is the set of admissible matchings (including boundary matches). The correction chain is lifted from paths corresponding to M^* .

Union-Find tracks cluster parity

$$\pi(C) = |C \cap \mathcal{X}| \bmod 2, \quad (6)$$

grows odd clusters, merges collisions, and peels spanning forests to produce a parity-consistent correction.

Neural-guided MWPM rescales matching weights via a trained model f_ϕ :

$$\tilde{w}_{ij} = \alpha_{ij} w_{ij}, \quad \alpha_{ij} = \text{clip}(f_\phi(x_{ij}), \alpha_{\min}, \alpha_{\max}), \quad (7)$$

then solves the same MWPM objective with \tilde{w} in place of w . This preserves the combinatorial decoder while changing edge priorities.

3. Logical-Error and Threshold Estimators

For code distance d , sweep parameter θ (either p or σ), and T trials with F logical failures,

$$\hat{p}_L(d, \theta) = \frac{F}{T}. \quad (8)$$

A standard normal-approximate 95% interval is

$$\hat{p}_L \pm 1.96 \sqrt{\frac{\hat{p}_L(1 - \hat{p}_L)}{T}}. \quad (9)$$

For two distances (d_a, d_b) on grid points θ_k , define

$$\Delta_k = \hat{p}_L(d_a, \theta_k) - \hat{p}_L(d_b, \theta_k). \quad (10)$$

If $\Delta_k \Delta_{k+1} < 0$, a linearized crossing estimate is

$$\hat{\theta}_c = \theta_k - \Delta_k \frac{\theta_{k+1} - \theta_k}{\Delta_{k+1} - \Delta_k}. \quad (11)$$

If no sign change exists on the sampled grid, the practical proxy is θ_{k^*} with

$$k^* = \arg \min_k |\Delta_k|. \quad (12)$$

For Pauli finite-size analysis, the standard collapse ansatz is

$$p_L(d, p) \approx f\left((p - p_c)d^{1/\nu}\right), \quad (13)$$

with (p_c, ν) obtained by minimizing a collapse cost over sampled curves and bootstrap resamples.

4. Deterministic Reproducibility Parameterization

Each run is indexed by (d, θ, t) with base seed s_0 . A deterministic seed map

$$s(d, \theta, t) = g(s_0, d, \theta, t) \quad (14)$$

guarantees identical pseudo-random streams for repeated executions under the same configuration. Together with fixed sweep sets

$$\begin{aligned} \mathcal{D} &= \{3, 5, 7\}, \\ \mathcal{P} &= \{0.04, 0.05, \dots, 0.12\}, \\ \Sigma &= \{0.05, 0.10, \dots, 0.60\}. \end{aligned} \quad (15)$$

this defines the reproducible experiment matrix used to generate all threshold and comparison tables in the paper.

-
- [1] A. Y. Kitaev, *Russian Mathematical Surveys* **52**, 1191 (1997).
- [2] D. Gottesman, A. Kitaev, and J. Preskill, *Physical Review A* **64**, 012310 (2001).
- [3] I. Tzitrin, T. Matsuura, R. N. Alexander, G. Dauphinais, J. E. Bourassa, K. K. Sabapathy, N. C. Menicucci, and I. Dhand, *PRX Quantum* **2**, 040353 (2021).
- [4] D. D. K. Wayo, *Lidmas: Architecture-level modeling of fault-tolerant magic-state injection in gkp photonic qubits* (2026), [arXiv:2601.16244 \[quant-ph\]](https://arxiv.org/abs/2601.16244).
- [5] O. Higgott and C. Gidney, *Quantum* **5**, 551 (2021).
- [6] N. Delfosse and N. H. Nickerson, *Quantum* **5**, 595 (2021), originally circulated as [arXiv:1709.06218](https://arxiv.org/abs/1709.06218) (2017).
- [7] J. P. Bonilla Ataides, D. K. Tuckett, S. D. Bartlett, S. T. Flammia, and B. J. Brown, *Nature Communications* **12**, 2172 (2021).
- [8] A. S. Darmawan, B. J. Brown, A. L. Grimsmo, D. K. Tuckett, and S. Puri, *PRX Quantum* **2**, 030345 (2021).
- [9] O. Higgott, T. C. Bohdanowicz, A. Kubica, S. T. Flammia, and E. T. Campbell, *Physical Review X* **13**, 031007 (2023).
- [10] L. Skoric, D. E. Browne, K. M. Barnes, N. I. Gillespie, and E. T. Campbell, *Nature Communications* **14**, 7040 (2023).
- [11] X. Tan, F. Zhang, R. Chao, Y. Shi, and J. Chen, *PRX Quantum* **4**, 040344 (2023).
- [12] Q. Xu, N. Mannucci, A. Seif, A. Kubica, S. T. Flammia, and L. Jiang, *Physical Review Research* **5**, 013035 (2023).
- [13] A. Dua, A. Kubica, L. Jiang, S. T. Flammia, and M. J. Gullans, *PRX Quantum* **5**, 010347 (2024).
- [14] R. Kobayashi and G. Zhu, *PRX Quantum* **5**, 020360 (2024).
- [15] K. Sahay, Y. Lin, S. Huang, K. R. Brown, and S. Puri, *PRX Quantum* **6**, 020326 (2025).
- [16] Y. Kang, J. Lee, J. Ha, and J. Heo, *Quantum Information Processing* **23**, 190 (2024).
- [17] J. Ha, Y. Kang, J. Lee, and J. Heo, *Quantum Information Processing* **24**, 164 (2025).
- [18] Y. Zhao, Y. Liu, C. Zhang, and et al., *Physical Review Letters* **129**, 030501 (2022).
- [19] S. Krinner, N. Lacroix, A. Remm, and et al., *Nature* **605**, 669 (2022).
- [20] K. Takeda, A. Noiri, T. Nakajima, T. Kobayashi, and S. Tarucha, *Nature* **608**, 682 (2022).
- [21] Z. Ni, S. Li, X. Deng, and et al., *Nature* **616**, 56 (2023).
- [22] Google Quantum AI, *Nature* **614**, 676 (2023).
- [23] U. Réglade, A. Bocquet, R. Gautier, and et al., *Nature* **629**, 778 (2024).
- [24] A. Z. Ding, B. L. Brock, A. Eickbusch, and et al., *Nature Communications* **16**, 5279 (2025).
- [25] Google Quantum AI and Collaborators, *Nature* **638**, 920 (2025).
- [26] S. C. Smith, B. J. Brown, and S. D. Bartlett, *Communications Physics* **7**, 386 (2024).
- [27] S. Bravyi, A. W. Cross, J. M. Gambetta, D. Maslov, P. Rall, and T. J. Yoder, *Nature* **627**, 778 (2024).
- [28] Q. Xu, G. Zheng, Y.-X. Wang, P. Zoller, A. A. Clerk, and L. Jiang, *npj Quantum Information* **9**, 78 (2023).
- [29] D. S. Wang, A. G. Fowler, and L. C. L. Hollenberg, *Physical Review A* **83**, 020302 (2011).
- [30] A. G. Fowler, *Physical Review Letters* **109**, 180502 (2012).
- [31] D. K. Tuckett, S. D. Bartlett, and S. T. Flammia, *Physical Review Letters* **120**, 050505 (2018).
- [32] D. K. Tuckett, S. D. Bartlett, S. T. Flammia, and B. J. Brown, *Physical Review Letters* **124**, 130501 (2020).
- [33] J. Lee, J. Park, and J. Heo, *Quantum Information Processing* **20**, 231 (2021).